Computers and Structures 123 (2013) 93–105

Contents lists available at SciVerse ScienceDirect

Computers and Structures

journal homepage: www.elsevier.com/locate/compstruc

Performance of an implicit time integration scheme in the analysis of wave propagations

Gunwoo Noh, Seounghyun Ham, Klaus-Jürgen Bathe *

Massachusetts Institute of Technology, Cambridge, MA 02139, United States

ARTICLE INFO

Article history:
Received 11 December 2012
Accepted 14 February 2013
Available online 27 March 2013

Keywords:
Wave propagation
Finite elements
Numerical dispersion
Implicit time integration
Newmark trapezoidal rule
Bathe method

ABSTRACT

In earlier work an effective implicit time integration scheme was proposed for the finite element solution of nonlinear dynamic problems [1,2]. The method, referred to as the Bathe method, was shown to possess unusual stability and accuracy characteristics for the solution of problems in linear and nonlinear structural dynamics [1–3]. In this paper we study the dispersion properties of the method, in comparison to those of the widely used Newmark trapezoidal rule, and show that the desired characteristics of the Bathe method for structural dynamics are also seen, and are very important, in the solution of wave propagation problems. A dispersion analysis is given and problems are solved to illustrate the capabilities of the scheme for the solution of wave propagation problems.

1. Introduction

Direct time integration is widely used in the finite element solutions of transient wave propagation problems, see e.g. [4,5]. However, accurate solutions are difficult to obtain because of numerical dispersion and dissipation, resulting from period elongations and amplitude decays [4–11]. Spurious oscillations, especially for high wave numbers, can severely ruin the accuracy of the solution. As waves travel, the errors from the difference between the numerical and analytically exact wave velocities, and their amplitudes, accumulate and the numerical solution can become very erroneous.

Much research effort has been focused on establishing techniques that reduce the dispersion and dissipation errors. Of course, by improving the spatial discretization, the solution can be more accurate. Most straightforwardly, a fine mesh with a very small time step size can be used. This strategy requires that the time step be selected carefully, depending on the element size, otherwise the solution errors are large even with a fine mesh [4,12,13]. Instead of a finer mesh, a higher-order spatial discretization [14–23] may be used to improve the solution accuracy. However, the use of higher-order elements can be computationally expensive and may not have the generality of the traditional finite element procedures using low order elements.

In the solution of transient wave propagations, the errors from the spatial and temporal discretizations appear together and affect each other [24–29]. Analyses of these errors have led to the use of linear combinations of consistent and lumped mass matrices [25,30–34]. Such approach can significantly reduce the dispersion error in one-dimensional analyses, but good accuracy in higher dimensional general wave propagations by this technique alone is difficult to reach.

Another approach is to reduce the solution errors by evaluating the mass and stiffness matrices using modified spatial integration rules [29,34,35]. Such schemes can improve the accuracy of solutions of multi-dimensional wave propagation problems when using certain elements and meshes. However, different integration rules than those commonly employed in static analyses have been proposed, and these rules may also depend on the material properties and CFL number used, which renders the approach not very practical.

The wave propagation solutions can also be improved by filtering spurious modes [34,36,37]. However, the filters are only applicable to specific points in space and time. Therefore, these techniques do not lend themselves to analyses where we want to see the solution for all times and over the complete solution domain (to, for example, make a movie of the calculated displacements and stresses).

Many direct time integration schemes introduce numerical dissipation to improve the solution by suppressing the high frequency spurious wave modes [4,38,39]. Such schemes do not require any additional computational effort and can be used for structural dynamics and wave propagation problems in a uniform manner [40]. However, to reach accurate solutions in wave propagation problems, the introduced numerical dissipation should be large enough to suppress the high frequency spurious waves while

* Corresponding author.
E-mail address: kjb@mit.edu (K.-J. Bathe).

0045-7949/$ - see front matter © 2013 Elsevier Ltd. All rights reserved.
http://dx.doi.org/10.1016/j.compstruc.2013.02.006

retaining good accuracy for the low frequency waves. Also, ideally, the solution procedure does not use any adjustable parameters, except that when employing the integration scheme, of course, an appropriate time step size needs to be used. These are the same desirable properties for a time integration scheme to be used in structural dynamics [2–4]. However, the spatial discretization and the time step size are chosen differently in structural dynamics and wave propagation analyses, as described in Ref. [4]. Notably, in wave propagation analyses, the time step size and the spatial discretization should be determined by considering the dispersion errors introduced by the spatial and temporal discretizations.

The Bathe time integration method has been shown to be very effective in linear and nonlinear structural dynamics [1–3,41]. The objective of this paper is to present a study of the scheme and show that the method is, indeed, also quite effective in the solution of wave propagation problems. In the following, we study the dispersion properties of the Bathe method and the Newmark trapezoidal rule (also herein referred to simply as trapezoidal rule) using 2-node and 4-node elements in one- and two-dimensional (1D and 2D) analyses. Based on the dispersion analysis, and the accuracy obtained in the wave modes that need to be represented accurately, we show that the properties of the Bathe scheme, valuable for structural dynamics, are also valuable for the solution of wave propagation problems. Finally, to illustrate our findings, we give the solutions of various problems using the Newmark trapezoidal rule and the Bathe method. While we consider in this paper only linear analysis, since the Bathe method is used without parameters to be adjusted [1–3], the conclusions reached here are directly applicable and are also of much value when considering nonlinear analyses.

2. A dispersion analysis

In this section, we analyse the dispersion errors resulting from the spatial discretization coupled with the temporal discretization. We consider the Bathe method and the Newmark trapezoidal rule. For this purpose, we analyse the solution obtained for the scalar wave governed by

$$\frac{\partial^2 u}{\partial t^2} - c_0^2 \nabla^2 u = 0 \tag{1}$$

where u is the field variable and c_0 is the wave velocity. Here, body forces are not considered since we focus on the dispersion associated with the propagations of disturbances due to initial conditions. The associated finite element discretization gives [4]

$$\mathbf{M}\ddot{\mathbf{U}} + c_0^2 \mathbf{K}\mathbf{U} = \mathbf{0} \tag{2}$$

where $\mathbf{K}$ and $\mathbf{M}$ are the stiffness and mass matrices, and for element (m) with volume $V^{(m)}$

$$\mathbf{M}^{(m)} = \int_{V^{(m)}} \mathbf{H}^{(m)^T} \mathbf{H}^{(m)} dV^{(m)} \tag{3}$$

$$\mathbf{K}^{(m)} = \int_{V^{(m)}} (\nabla \mathbf{H}^{(m)})^T (\nabla \mathbf{H}^{(m)}) dV^{(m)} \tag{4}$$

Here $\mathbf{H}^{(m)}$ and $\mathbf{U}$ are the element interpolation matrix and the nodal values of the solution, respectively. The matrices $\mathbf{M}$ and $\mathbf{K}$ in Eq. (2) are obtained by the usual summation process [4]. In the actual evaluations, we use a unit cross-sectional area in 1D solutions and a unit thickness in 2D solutions in accordance with Eq. (1). Note that we use the 'consistent' mass matrix in the solutions.

In the Bathe method, the following relations are employed [2]

$${}^{t+\Delta t/2}\dot{\mathbf{U}} = {}^{t}\dot{\mathbf{U}} + \left[\frac{\Delta t}{4}\right]({}^{t}\ddot{\mathbf{U}} + {}^{t+\Delta t/2}\ddot{\mathbf{U}}) \tag{5}$$

$${}^{t+\Delta t/2}\mathbf{U} = {}^{t}\mathbf{U} + \left[\frac{\Delta t}{4}\right]({}^{t}\dot{\mathbf{U}} + {}^{t+\Delta t/2}\dot{\mathbf{U}}) \tag{6}$$

$${}^{t+\Delta t}\dot{\mathbf{U}} = \frac{1}{\Delta t}{}^{t}\mathbf{U} - \frac{4}{\Delta t}{}^{t+\Delta t/2}\mathbf{U} + \frac{3}{\Delta t}{}^{t+\Delta t}\mathbf{U} \tag{7}$$

$${}^{t+\Delta t}\ddot{\mathbf{U}} = \frac{1}{\Delta t}{}^{t}\dot{\mathbf{U}} - \frac{4}{\Delta t}{}^{t+\Delta t/2}\dot{\mathbf{U}} + \frac{3}{\Delta t}{}^{t+\Delta t}\dot{\mathbf{U}} \tag{8}$$

Using Eq. (2) at times t, $t + \Delta t/2$ and $t + \Delta t$, where t denotes the current time and Δt the time step, with Eqs. (5)–(8), we obtain a linear multistep form of the Bathe method

$$(72\mathbf{M} + 8c_0^2\Delta t^2\mathbf{K})^{t+\Delta t}\mathbf{U} + (-144\mathbf{M} + 5c_0^2\Delta t^2\mathbf{K})^{t+\Delta t/2}\mathbf{U} + (72\mathbf{M} + 5c_0^2\Delta t^2\mathbf{K})^{t}\mathbf{U} = \mathbf{0} \tag{9}$$

Using the definition of the CFL number, $\mathrm{CFL} = \frac{c_0\Delta t}{h}$, where h is the 'characteristic length' of a finite element (or fundamental length used) [4], Eq. (9) becomes

$$(72\mathbf{M} + 8\gamma\mathbf{K})^{t+\Delta t}\mathbf{U} + (-144\mathbf{M} + 5\gamma\mathbf{K})^{t+\Delta t/2}\mathbf{U} + (72\mathbf{M} + 5\gamma\mathbf{K})^{t}\mathbf{U} = \mathbf{0} \tag{10}$$

where $\gamma = \mathrm{CFL}^2 h^2$.

In the Newmark method, the equations used are [4]

$${}^{t+\Delta t}\dot{\mathbf{U}} = {}^{t}\dot{\mathbf{U}} + [(1-\delta){}^{t}\ddot{\mathbf{U}} + \delta^{t+\Delta t}\ddot{\mathbf{U}}]\Delta t \tag{11}$$

$${}^{t+\Delta t}\mathbf{U} = {}^{t}\mathbf{U} + {}^{t}\dot{\mathbf{U}}\Delta t + \left[\left(\frac{1}{2} - \alpha\right){}^{t}\ddot{\mathbf{U}} + \alpha^{t+\Delta t}\ddot{\mathbf{U}}\right]\Delta t^2 \tag{12}$$

where α and δ are the Newmark parameters. Using Eq. (2) for the equilibrium at times $t - \Delta t$, t and $t + \Delta t$ with Eqs. (11) and (12) we obtain, for the case $\delta = 1/2$, the linear multistep form of the Newmark method

$$(\mathbf{M} + \alpha c_0^2\Delta t^2\mathbf{K})^{t+\Delta t}\mathbf{U} + (-2\mathbf{M} + (1-2\alpha)c_0^2\Delta t^2\mathbf{K})^{t}\mathbf{U} + (\mathbf{M} + \alpha c_0^2\Delta t^2\mathbf{K})^{t-\Delta t}\mathbf{U} = \mathbf{0} \tag{13}$$

or,

$$(\mathbf{M} + \alpha\gamma\mathbf{K})^{t+\Delta t}\mathbf{U} + (-2\mathbf{M} + (1-2\alpha)\gamma\mathbf{K})^{t}\mathbf{U} + (\mathbf{M} + \alpha\gamma\mathbf{K})^{t-\Delta t}\mathbf{U} = \mathbf{0} \tag{14}$$

Then setting $\alpha = 1/4$ we obtain the equations for the Newmark trapezoidal rule. It appears here that the computational effort in the Bathe method is twice that used in the Newmark method (because in the Bathe method, the solution at the half step is used), but we shall see that this is not the case when solutions of optimal accuracy are sought (see Section 3.1).

2.1. A dispersion error analysis in the 1D case

In the one-dimensional case, the general solution of Eq. (1), for one wave traveling along the coordinate x, has the form of $Ae^{i(k_0x-\omega_0t)}$, where ω_0 is the frequency of the wave mode and $k_0 = \omega_0/c_0$ is the corresponding wave number. The numerical solution takes in general the form [29]

$${}^{t}_{x}u = A_k e^{i(kx-\omega t)} \tag{15}$$

where ω and $k = \omega/c$ are the numerical frequency and the corresponding wave number, respectively. The numerical wave speed c is different from the exact wave speed c_0, and the difference is a function of the wave number; therefore, this difference results in general analysis in artificial dispersion. In addition, we have that, for unconditionally stable implicit methods (in linear analysis), the amplitude of the wave as numerically calculated usually decreases due to numerical damping [4]. An exception is the Newmark trapezoidal rule, where this damping effect is not present. As we

shall see below, the Bathe method does possess the damping property in such a way that surprisingly accurate solutions are obtained.

We now consider a regular mesh with nodes equally spaced Δx apart along the x axis, then the solution to the finite element system at time $n_t\Delta t$ and location $n_x\Delta x$ is

$$ {}^{n_t\Delta t}_{n_x\Delta x}u = A_k e^{i(kn_x\Delta x - \omega n_t\Delta t)} = A_k e^{ik\Delta x(n_x - n_t(\mathrm{CFL})(c/c_0))} \tag{16} $$

where the subscript and superscript denote the nodal value at $n_x\Delta x$ and time $n_t\Delta t$.

For the 2-node element, the corresponding mass matrix **M** and stiffness matrix **K** of the finite element equations are

$$ \mathbf{M} = \frac{\Delta x}{6}\begin{pmatrix} 2 & 1 & 0 & & \cdots & 0 \\ 1 & 4 & 1 & & \cdots & 0 \\ 0 & 1 & 4 & 1 & & \vdots \\ \vdots & & & \ddots & & \vdots \\ 0 & \cdots & \cdots & & 1 & 2 \end{pmatrix} \tag{17} $$

$$ \mathbf{K} = \frac{1}{\Delta x}\begin{pmatrix} 1 & -1 & 0 & & \cdots & 0 \\ -1 & 2 & -1 & & \cdots & 0 \\ 0 & -1 & 2 & -1 & & \vdots \\ \vdots & & & \ddots & & \vdots \\ 0 & \cdots & \cdots & & -1 & 1 \end{pmatrix} \tag{18} $$

Now substituting from Eqs. (16)–(18) into Eq. (10) with $h = \Delta x$, and considering the equation of the middle node of a two element patch, we obtain for the Bathe method a relation between the values of the CFL number $= \frac{c_0\Delta t}{\Delta x}$, c/c_0, wave number k, and the element size Δx. The results are given in Fig. 1 in terms of the wavelength λ and the element size used.

As seen in Fig. 1, there is no CFL number that makes every wave mode have the same wave speed. However, an important property seen in Fig. 1 is that using CFL = 1, we will have all wave modes with $k\Delta x < 2$ to be almost non-dispersive, whereas all higher frequency modes have dispersion. These higher frequency modes should therefore not be included in a solution that contains many wave modes and that can be approximated by only using the wave modes $k\Delta x < 2$.

This is indeed accomplished when using the Bathe method: the wave modes with $\Delta t/T > 0.3$, where T is the wave period, are in essence discarded in the numerical solution due to numerical damping [3]. Namely, using the definition of the CFL number, we can rewrite $k\Delta x$ in terms of $\Delta t/T$ as

$$ k\Delta x = 2\pi\frac{c_0}{c}\frac{1}{\mathrm{CFL}}\frac{\Delta t}{T} \tag{19} $$

Therefore, for CFL $\simeq 1$, since the numerical wave speed is approximately equal to the exact wave speed, that is, we can use $c/c_0 \simeq 1$, we see that wave modes with $k\Delta x \gtrsim 0.6\pi$ are not participating in the total solution (these discarded wave modes are presented as dotted lines in Fig. 1 for various CFL numbers). The important point to notice is that with CFL = 1, the Bathe method solves for *every participating wave mode very accurately* so that the total solution is almost non-dispersive.

For the Newmark trapezoidal rule, using Eqs. (16)–(18) and (14) with $h = \Delta x$, and considering the equation corresponding to the middle node of a two element patch, we obtain the relation between the values of CFL, c/c_0, wave number k, and the element size Δx shown in Fig. 2. The wave modes with $k\Delta x < 2$ become almost non-dispersive with CFL = 0.65. However, wave modes with $k\Delta x > 2$ are dispersive, because they are not damped out, see Fig. 2. Therefore, as in the Bathe method, there is no CFL number which makes the solution from all participating wave modes non-dispersive – but different from the Bathe method, the trapezoidal rule does not eliminate the dispersive modes from the solution. Hence the solution will generally show a significant dispersion error, as shown for specific examples in Section 3, where also the CFL numbers 1.0 for the Bathe method and 0.65 for the trapezoidal rule are discussed as being the optimal numbers to use.

We focused here on the dispersion properties of the methods. However, it should be noted that for an accurate solution of wave propagation problems, it is also necessary to have good solution accuracy in the calculation of the wave modes that are participating in the response. Therefore, time integration methods that have good spectral radii curves might produce good dispersion characteristics, but might not be effective because the errors in the calculation of the low modes are too large, see Figs. 3–5 [3,4,42–44].

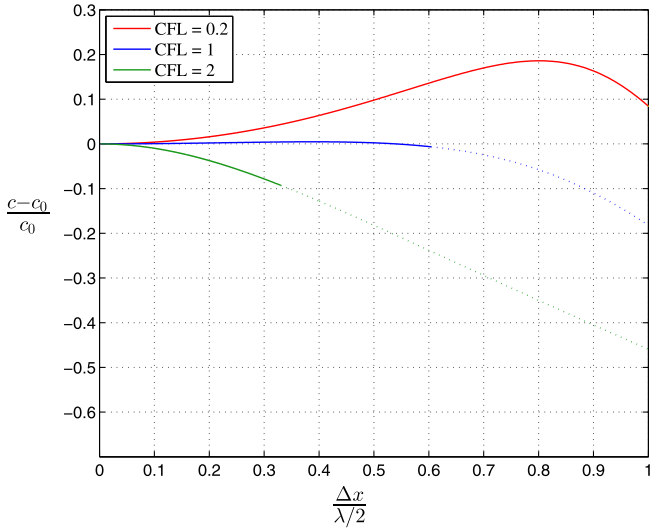

Fig. 1. Relative wave speed errors of the Bathe method for various CFL numbers; results for discarded wave modes are given by dotted lines.

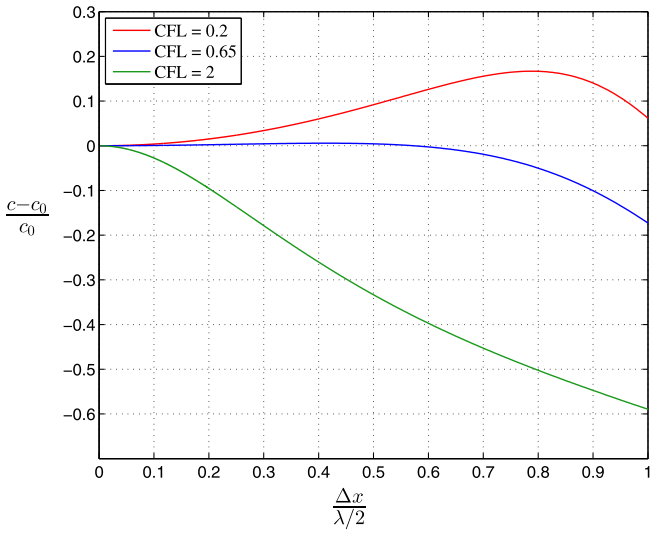

Fig. 2. Relative wave speed errors of the trapezoidal rule for various CFL numbers.

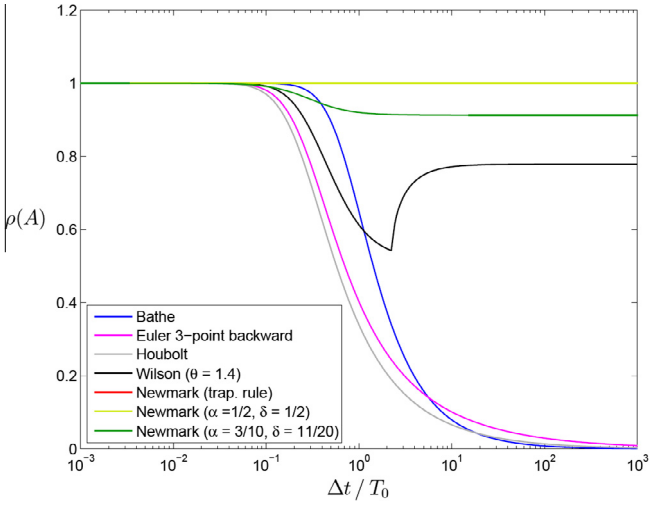

Fig. 3. Spectral radii of approximation operators, case $\xi = 0$, for various methods; $\rho(A) = 1.0$ for the Newmark trap. rule and when $\alpha = 1/2$, $\delta = 1/2$ in the Newmark method.

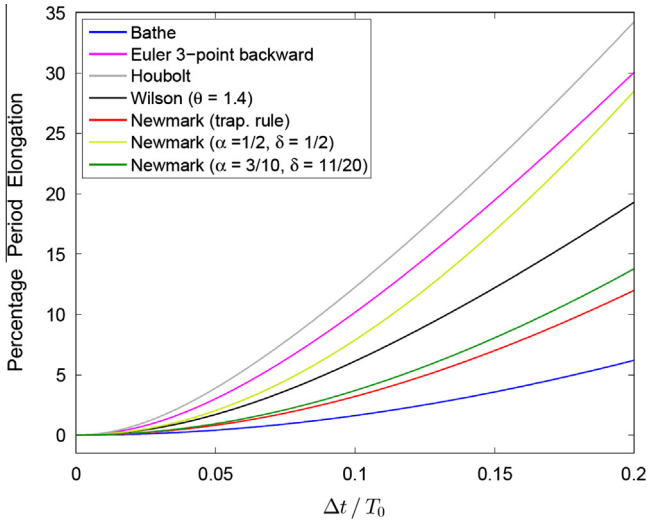

Fig. 4. Percentage period elongations for various methods.

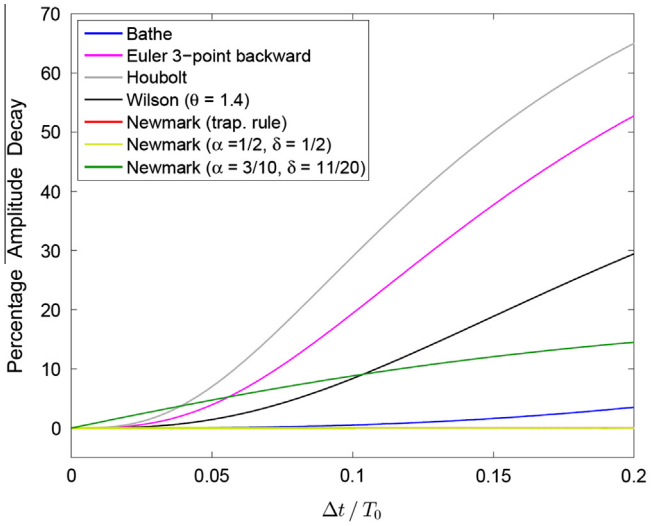

Fig. 5. Percentage amplitude decays for various methods; results for Newmark (trap. rule) and Newmark ($\alpha = 1/2$, $\delta = 1/2$) are identical.

2.2. A dispersion error analysis for the 2D case

In two-dimensional analyses, the general solution of Eq. (1) for a plane wave is given by $u = A\, e^{i(k_0 x\cos(\theta)+k_0 y\sin(\theta)-\omega_0 t)}$, and the corresponding numerical solution is

$$ {}^{t}_{x,y}u = A_k e^{i(kx\cos(\theta)+ky\sin(\theta)-\omega t)} \tag{20}$$

For a mesh with nodes equally spaced with distance h along both x and y axes ($\Delta x = \Delta y = h$), the solution of the finite element system at time $n_t\Delta t$ and location $n_x h$, $n_y h$ is

$$\begin{aligned} {}^{n_t\Delta t}_{n_x h, n_y h}u &= A_k e^{i(kn_x h\cos(\theta)+kn_y h\sin(\theta)-\omega n_t\Delta t)} \\ &= A_k e^{ikh(n_x\cos(\theta)+n_y\sin(\theta)-n_t(\mathrm{CFL})(c/c_0))} \end{aligned} \tag{21}$$

where θ is the angle, from the x-axis, at which the wave is propagating.

As in the 1D case, substituting the above expression into the linear multistep formula, and looking at the equation corresponding to the middle node of a patch of elements, which now consists of four square finite elements, we obtain a relation between $\mathrm{CFL} = c_0\Delta t/h$, c/c_0, the wave number k, and the element size h.

For the four-node element, the row of the global mass matrix corresponding to the middle node at (x,y) is

$$\frac{h^2}{36}[0\cdots 0\ 1\ 4\ 1\ 4\ 16\ 4\ 1\ 4\ 1\ 0\ \cdots\ 0] \tag{22}$$

Therefore, the $\mathbf{M}^t\mathbf{U}$ term for the node at (x,y) is

$$\begin{aligned} &\frac{h^2}{36}\Big[16\,{}_{x,y}{}^{t}u + 4\Big({}_{x-h,y}{}^{t}u + {}_{x+h,y}{}^{t}u + {}_{x,y-h}{}^{t}u + {}_{x,y+h}{}^{t}u\Big) \\ &\quad + \Big({}_{x-h,y-h}{}^{t}u + {}_{x+h,y-h}{}^{t}u + {}_{x-h,y+h}{}^{t}u + {}_{x+h,y+h}{}^{t}u\Big)\Big] \end{aligned} \tag{23}$$

Also, the corresponding row of the global stiffness matrix $\mathbf{K}$ is

$$\frac{1}{3}[0\cdots\ 0\ -1\ -1\ -1\ -1\ 8\ -1\ -1\ -1\ -1\ 0\cdots 0] \tag{24}$$

Therefore, the $\mathbf{K}^t\mathbf{U}$ term for the node is

$$\begin{aligned} &\frac{1}{3}\Big[8\,{}_{x,y}{}^{t}u - \Big({}_{x-h,y}{}^{t}u + {}_{x+h,y}{}^{t}u + {}_{x,y-h}{}^{t}u + {}_{x,y+h}{}^{t}u + {}_{x-h,y-h}{}^{t}u \\ &\quad + {}_{x+h,y-h}{}^{t}u + {}_{x-h,y+h}{}^{t}u + {}_{x+h,y+h}{}^{t}u\Big)\Big] \end{aligned} \tag{25}$$

Using Eqs. (21), (23), (25), and (10), we obtain for the Bathe method the results for various propagating angles shown in Fig. 6(a). As in the 1D case, there is no CFL number that makes every wave mode have the same wave speed.

Of course, the dispersion error depends on the propagating angle. As seen, the Bathe method cuts the highly dispersive parts off effectively, and for the case CFL = 1, the largest dispersion error is less than 6%, for the direction $\pi/4$ (Fig. 6(a)).

An interesting point is that for a larger angle of propagation, lower curves are seen in Fig. 6. We observed a similar trend in the 1D analysis – a larger CFL number results in a lower curve in Figs. 1 and 2. Therefore, larger angles of propagation introduce errors in the same way as larger CFL numbers for a given $c_0\Delta t$; in other words, waves propagating at a non-zero angle behave as if the element size were *shorter* than h.

Indeed for waves with propagating angle θ, the CFL number that results into the smallest dispersion error can be estimated from the expression (obtained with some arithmetic)

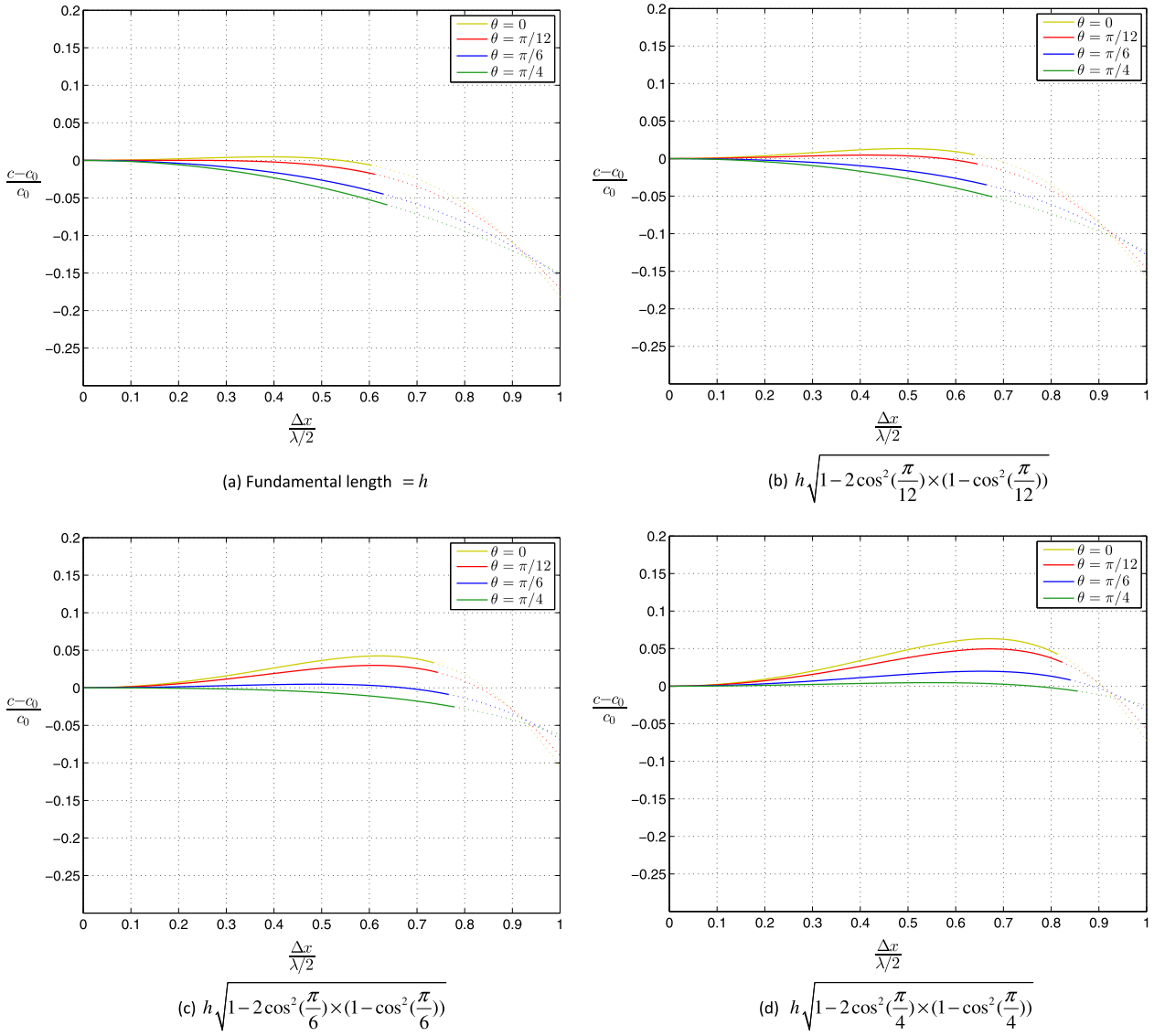

Fig. 6. Relative wave speed errors of the Bathe method for various propagating angles, using CFL = 1, calculated for various effective fundamental lengths; results for discarded wave modes are shown by dotted lines.

$$\frac{c-c_0}{c_0} = -\frac{1}{1152}(96(\cos^2\theta - \cos^4\theta) + 41\mathrm{CFL}^2 - 48)(kh)^2 + O((kh)^4) \tag{26}$$

From this expression we can identify that an approximate optimal CFL value is 1.0 when $\theta = 0$ and we use this CFL number also when the angle is greater than zero. For values of $\theta > 0$, we calculate the time step size Δt by holding CFL = 1 and considering the *effective* fundamental length to be $h \times \sqrt{1 - 2\cos^2\theta(1 - \cos^2\theta)}$. Note that, as intuition might also suggest, to obtain the best results when the wave is propagating at the angle $\pi/4$, we should consider the element fundamental length to be $h/\sqrt{2}$ and not $\sqrt{2}h$.

Fig. 6 shows the dispersion characteristic curves of the Bathe method with CFL = 1 for various propagating angles and for various fundamental lengths. For each case, the solution accuracy of the wave with the propagating angle is excellent when the optimum effective element length is used.

For the Newmark trapezoidal rule, we obtain the dispersion relation from Eqs. (21), (23), (25), and (14), and for $\theta = 0$, the best CFL number is identified to be 0.65. The results when using CFL = 0.65 are shown in Fig. 7(a), and we note again that the trapezoidal rule also has no CFL number which makes every wave mode have the same propagating speed.

The dispersion error using the trapezoidal rule also depends upon the propagating angle since this effect is due to the spatial discretization. However, more severely, the dispersion error of shorter wavelength modes is quite large and these are participating in the total solution unlike in the Bathe method.

Also, as in the Bathe method, for the propagating angle θ, the effective element length is best reduced to $h \times \sqrt{1 - 2\cos^2\theta(1 - \cos^2\theta)}$. Fig. 7 shows the dispersion characteristic curves of the trapezoidal rule using CFL = 0.65 for various propagating angles and for various fundamental lengths. The error is reduced when the optimal effective element length is used.

However, we should note that in actual practical analyses, the wave will travel in all directions across elements, and hence a good rule is to choose at least six elements to represent the smallest important excited wavelength (see also Section 3.2).

3. Wave propagation solutions

In this section, we present the performance of the Bathe method in the solution of wave propagation problems through several numerical examples. First, we solve a one-dimensional impact

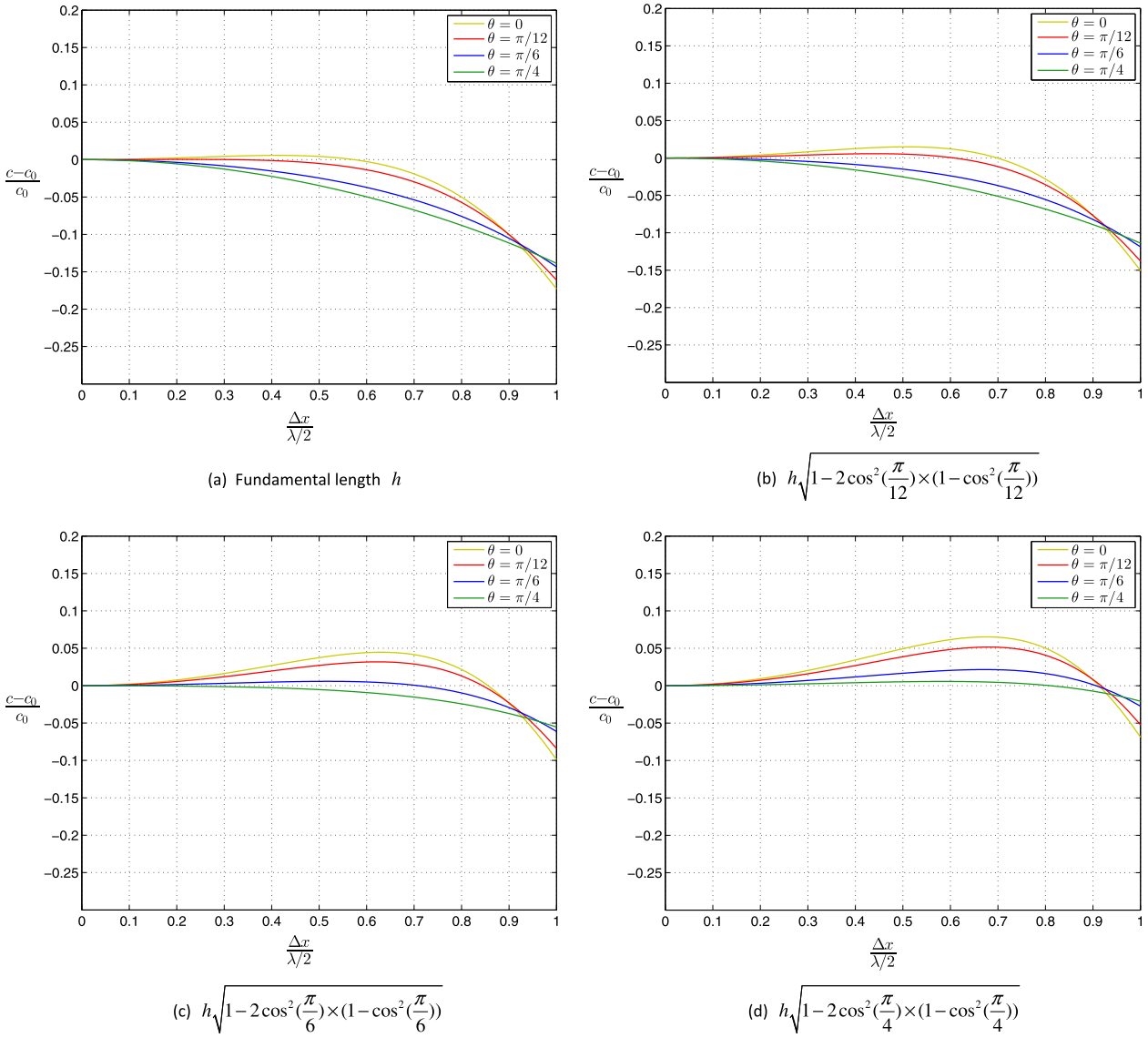

Fig. 7. Relative wave speed errors of the trapezoidal rule for various propagating angles, using CFL = 0.65, calculated for various effective fundamental lengths.

problem and focus on the influence of the CFL number on the numerical dispersion properties and the resulting spurious oscillations. We then solve a 2-D transient scalar wave problem and focus on the dispersion properties that depend on the propagating angle. Finally we solve a Lamb problem with two types of external loading using the Bathe method and the trapezoidal rule, and compare the results with the analytical solution.

3.1. 1-D bar impact

We consider the impact of an elastic bar on a rigid wall, see Fig. 8 for which the governing wave equation is

$$\frac{\partial^2 u}{\partial x^2} = \frac{1}{c_0^2}\frac{\partial^2 u}{\partial t^2} \tag{27}$$

For the material properties used, the wave speed c_0 is 5000. The elastic bar is idealized using 1-D 2-node elements of size $\Delta x = 0.05$.

For the solution, we use the Bathe method and the trapezoidal rule. We use the CFL numbers 0.2, 1, and 2 for the Bathe method, and the CFL numbers 0.2, 0.65, and 2 for the trapezoidal rule. For each scheme, the corresponding time step sizes are the CFL numbers multiplied by 10^{-5}.

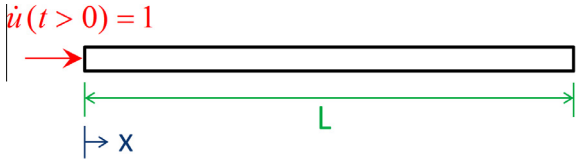

Fig. 8. 1D bar impact problem, $c_0 = 5000$; applied velocity at left end is 1 for time $t > 0$; initial displacement and velocity are zero.

Figs. 9–12 give the calculated results when the bar length is 10. As we see in Figs. 1 and 2, for CFL = 0.2, short wavelength modes have wave speeds faster than the analytical wave speed in both time integration methods. With this CFL number, oscillations mainly occur forward of the wave front for both methods. On the other hand, for CFL = 2, short wavelength modes have slower wave speeds for both schemes, and oscillations occur mainly behind the wave front and the slope of the wave front is decreased.

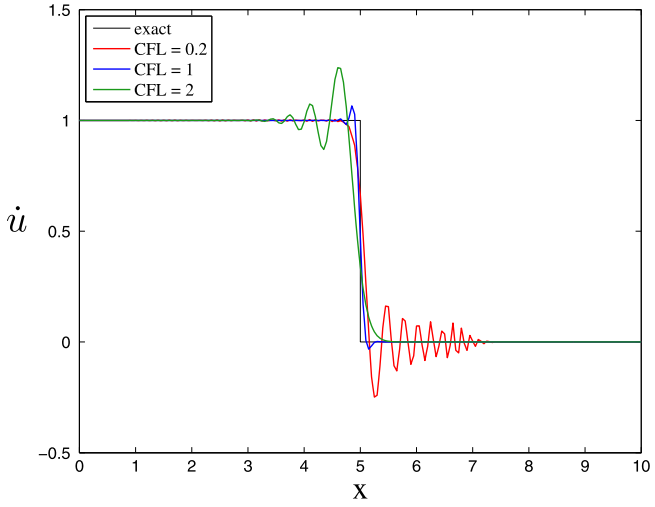

Fig. 9. Velocity distributions using the Bathe method with various CFL numbers.

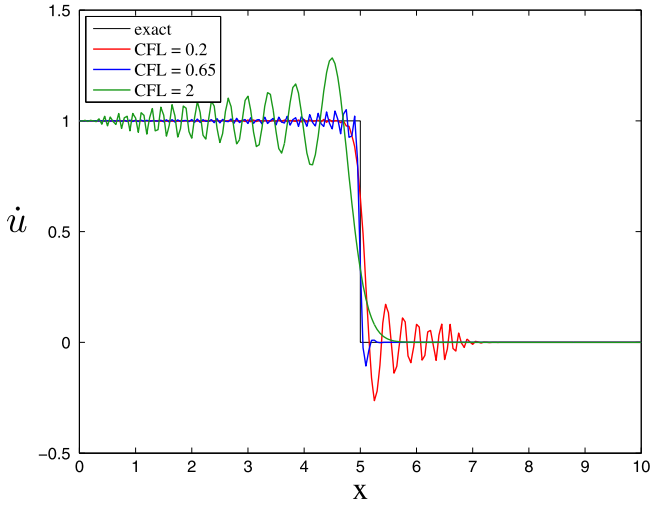

Fig. 10. Velocity distributions using the trapezoidal rule with various CFL numbers.

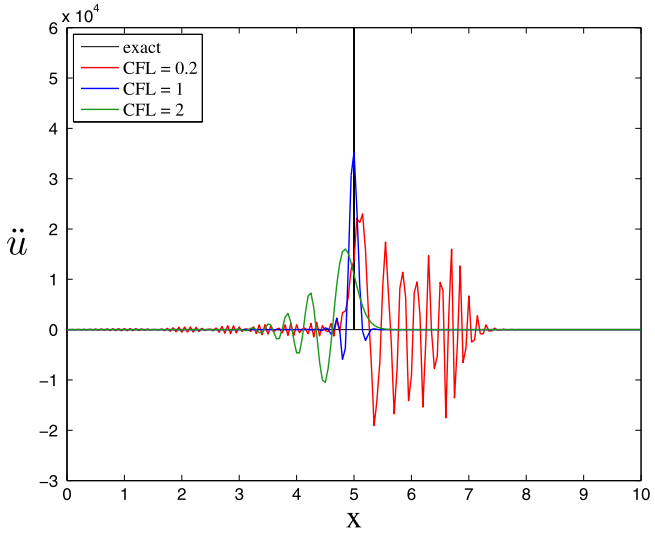

Fig. 11. Acceleration distributions using the Bathe method with various CFL numbers.

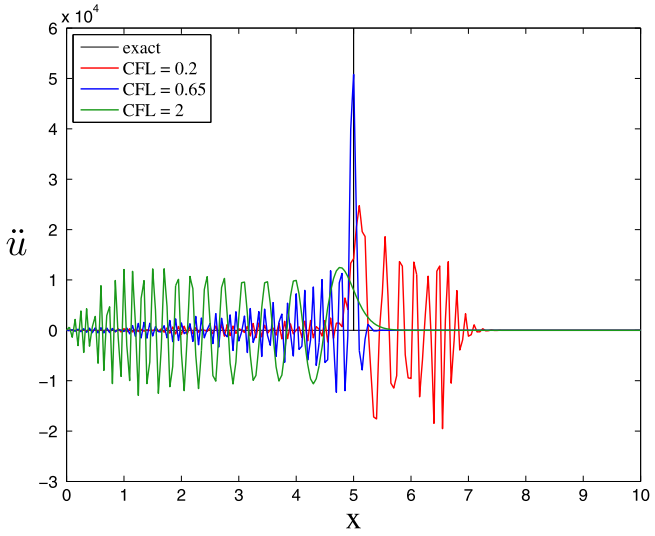

Fig. 12. Acceleration distributions using the trapezoidal rule with various CFL numbers.

While both methods give very similar solutions for CFL = 0.2, they perform quite differently for CFL = 2. The reason is that for CFL = 0.2, the dispersion property for both methods is similar, see the curves in Figs. 1 and 2, and in both methods wave modes that, spatially, can only be crudely approximated are not discarded.

However, for CFL = 2, the range of discarded wave modes in the Bathe method is obtained as $k\Delta x/\pi \gtrsim 2(\sim 1.1)(1/2)(\sim 0.3) \simeq 0.33$. Therefore, since the participating (effective) wave modes are significantly different, the total solutions from each method are also different.

An important point is that for CFL = 1, the Bathe method discards the wave modes with large wave speed error. As a result, only the modes with almost no wave speed error are participating in the total solution; therefore, the solution becomes almost non-dispersive. Of course, due to the loss of some high frequency modes, the Fourier truncation error is a little increased. Indeed, we observe that the effect of this increased truncation error is not significant (e.g., the slope of the wave front is only slightly decreased compared to the results obtained using the trapezoidal rule).

Since the solution using the Bathe method is not dispersive for CFL = 1, in this case the solution is very accurate for relatively long time simulations. Figs. 13 and 14 show the case of the bar length = 100 (the number of elements is 2000). In the figures, the results using the Bathe method with CFL = 1 and the trapezoidal rule with CFL = 0.65 are shown. The solution using the Bathe method is accurate. But when using the trapezoidal rule with CFL = 0.65, the accuracy of the solution decreases significantly as the wave propagates, due to the accumulation of the dispersion error.

Note that the CFL numbers 1 and 0.65 are also reported in Ref. [45] as those that give the smallest global errors at a certain observation time. Since when using CFL = 1, the Bathe method gives almost non-dispersive solutions, we would expect that a global error measure applied at any observation time will give that same result, that is, a good CFL number to use is 1.

Further, it is interesting to note that using these CFL numbers for the two schemes, the computational effort for the complete solution using the Bathe method is not much higher than when using the trapezoidal rule – while the increase in accuracy using the Bathe method is most important.

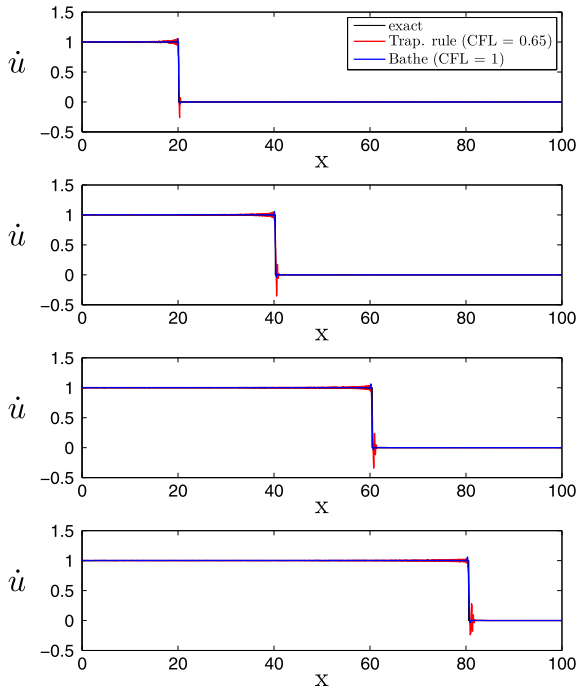

Fig. 13. Velocity distributions; blue line – Bathe method (CFL = 1); red line – Trapezoidal rule (CFL = 0.65); for various observation times. (For interpretation of the references to color in this figure legend, the reader is referred to the web version of this article.)

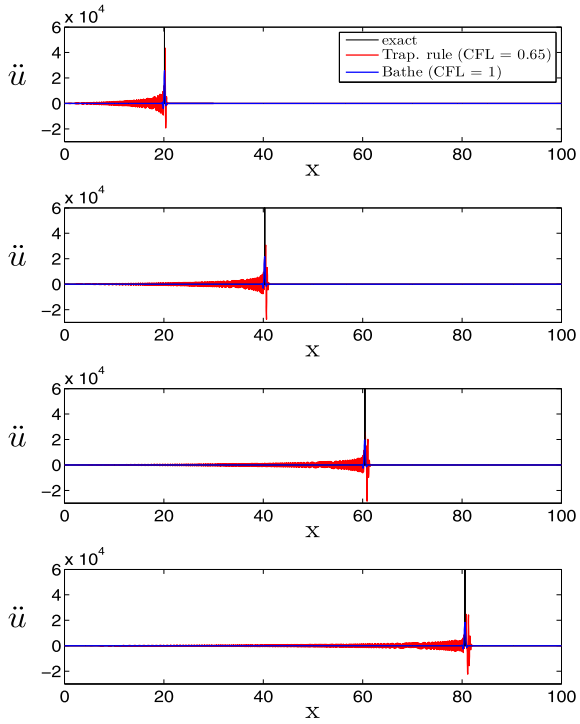

Fig. 14. Acceleration distributions; blue line – Bathe method (CFL = 1); red line – Trapezoidal rule (CFL = 0.65); for various observation times. (For interpretation of the references to color in this figure legend, the reader is referred to the web version of this article.)

3.2. 2D scalar wave propagation

Here we consider a pre-stressed membrane, see Fig. 15, for which the transverse displacement, u, is given by the equation

$$\frac{\partial^2 u}{\partial x^2}+\frac{\partial^2 u}{\partial y^2}+F(0,0,t)=\frac{1}{c_0^2}\frac{\partial^2 u}{\partial t^2} \tag{28}$$

where c_0 is the wave velocity, taken in this example equal to 1. The load is given as

$$F(0,0,t)=4(1-(2t-1)^2)H(1-t), \quad t>0 \tag{29}$$

where H is the unit step function. Only the domain, $[0,15]\times[0,15]$, is considered in the solution due to symmetry, and no absorbing boundary conditions are used since the wave does not propagate to the boundary for the solution time considered. The computational domain is idealized using six meshes of four-node elements. The Bathe method and the trapezoidal rule are used with the CFL numbers 1 and 0.65, respectively. For the CFL numbers, the lengths of the side of the elements are used as the fundamental length.

Figs. 16 and 17 show snapshots of the solution variable u, calculated using the Bathe method and the trapezoidal rule at $t = 13$ for various meshes. We observe that for low spatial discretization density, both methods give spurious oscillations. However, using the 75 by 75 element mesh, the Bathe method gives a reasonably accurate solution (see also Fig. 18) while the trapezoidal rule gives noticeable spurious oscillations and even still so when using the 165 by 165 element mesh.

In Figs. 18 and 19, numerical results at time $t = 13$ using the 75 by 75 mesh are compared with the analytical solution. The angles considered are 0 and $\pi/4$. The trapezoidal rule gives spurious oscillations. The solution for u at the angle of zero degrees using the Bathe method is quite accurate, but the method shows a significant solution error in predicting the peak value of $\dot{u}$. As expected, using the element side length as effective element length, the solutions using the Bathe method and the trapezoidal rule are less accurate for the response at $\pi/4$, see also Figs. 6 and 7. Figs. 20 and 21 show the same results using the 105 by 105 element mesh and it is seen that the accuracy of the solution using the Bathe method is quite improved.

Although the Bathe method significantly improves the solution, the dispersion curves and the results of this example indicate that waves propagating at nonzero angles to the element sides, require that in this analysis $\Delta x/(\lambda/2) \leqslant 0.2$.

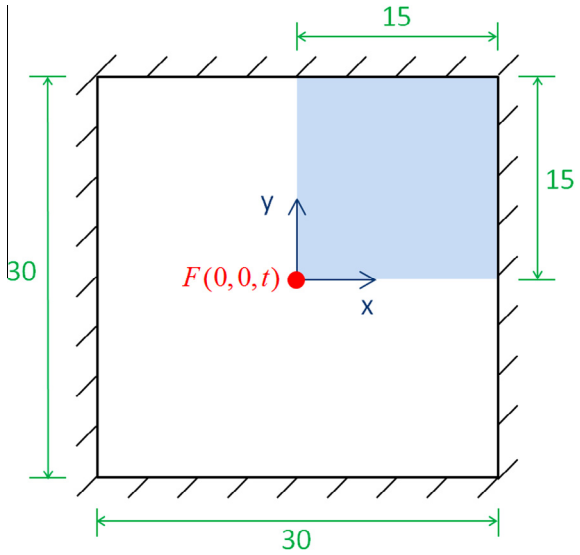

Fig. 15. Pre-stressed membrane problem, $c_0 = 1$, initial displacement and velocity are zero, computational domain is shaded.

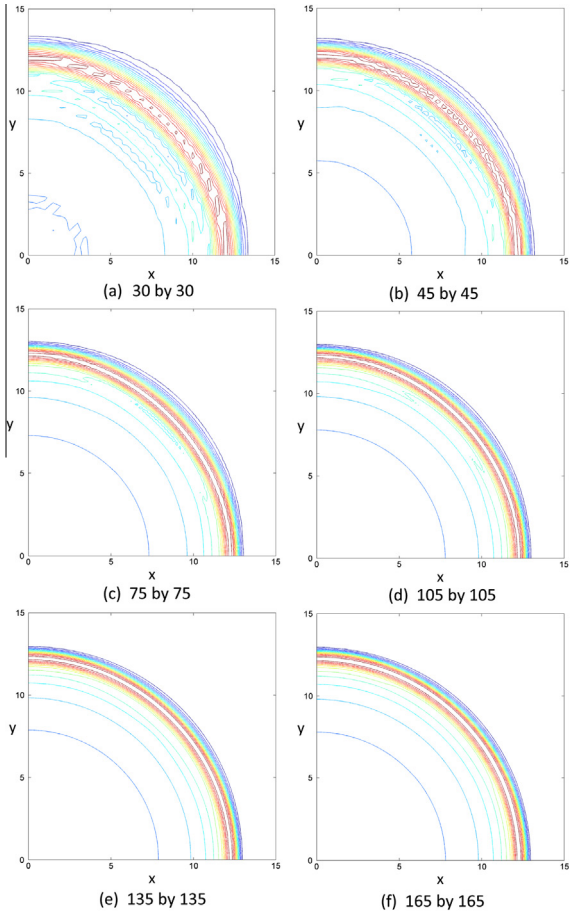

Fig. 16. Snapshots of displacements at time $t = 13$, Bathe method, CFL = 1; using various meshes.

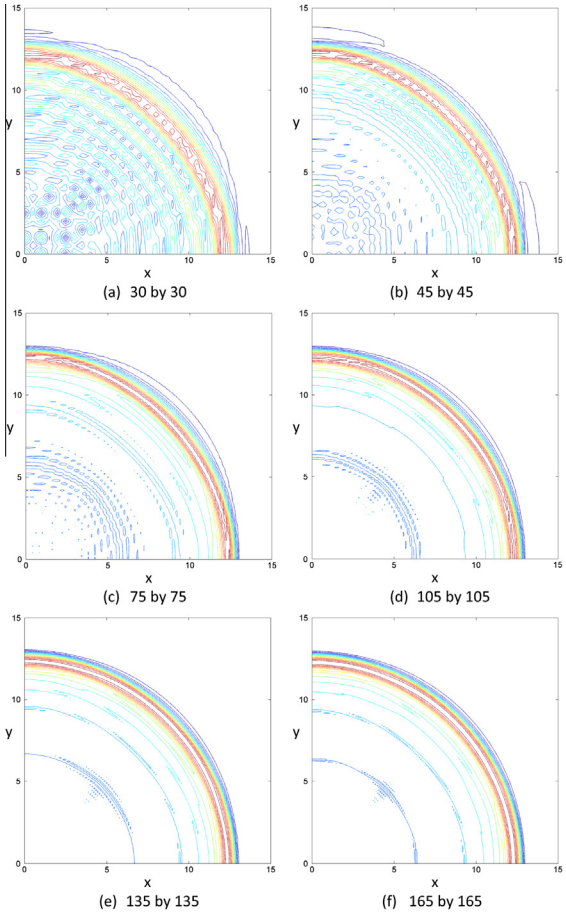

Fig. 17. Snapshots of displacements at time $t = 13$, trapezoidal rule, CFL = 0.65, using various meshes.

3.3. 2D elastic wave propagation

So far we considered scalar wave propagations that are characterized by a single wave speed. We obtained the appropriate time step sizes for each time integration method using the CFL numbers to minimize the numerical dispersion of the waves with the same phase velocity. However many physical problems are characterized by multiple wave speeds. As an example, we consider a Lamb problem, in which waves are propagating in a semi-infinite elastic domain in plane strain conditions [23].

The problem is described in Fig. 22. For the material properties used, we have the P-wave velocity = 3200 m/s, S-wave velocity = 1848 m/s, and the Rayleigh wave velocity = 1671 m/s. The time duration for computing the waves is 0.999 s, so that the P-wave does not reach the outer boundaries; hence it is not necessary to incorporate absorbing boundary conditions. Since we are mostly interested in the Rayleigh wave profile, we calculate the time step sizes based on the speed of the Rayleigh wave, and use the CFL numbers 1 and 0.65 for the Bathe method and the trapezoidal rule, respectively.

We first consider the line force, a Ricker wavelet, defined as

$$F(0,0,t) = -2\times 10^3 \times (1-2\pi^2\hat{f}^2(t-t_0)^2)\exp(-\pi^2\hat{f}^2(t-t_0)^2), \quad t>0 \tag{30}$$

where the central frequency $\hat{f} = 12.5$ Hz and $t_0 = 0.1$ s. In the solution we use symmetry and a domain with a mesh of 640×640 four-node elements of side lengths $\Delta x = \Delta y = 5$ m, see Fig. 22. Fig. 23 shows the calculated displacements at two receivers which are located at $x = 640$ m and $x = 1280$ m from the source. The analytical solution and the numerical solutions using the Bathe method and the trapezoidal rule are plotted. The numerical solutions using both methods are in good agreement with the analytical solution.

Since this load type can be well approximated with only a few harmonic functions, there are a limited number of wave modes that are excited. Therefore, if we use a fine mesh so that all excited wave modes are within $\Delta x/(\lambda/2) \leqslant 0.2$ as done here, both, the Bathe method and the trapezoidal rule give very accurate solutions. Fig. 24 shows the calculated stress field at time $t = 0.9196$. Color bars in Fig. 24 indicate the magnitude of the von Mises stress.

We next consider the line force defined as

$$F(0,0,t) = 2\times 10^3 \times [H(0.15-t) - 3H(0.1-t) + 3H(0.05-t)], \quad t>0 \tag{31}$$

where H is the unit step function. The load consists now of three step functions which renders the problem more difficult to solve numerically. The computational domain is now discretized using a mesh of 1600×1600 4-node elements of side lengths $\Delta x = \Delta y = 2$ m. In Fig. 25 we see displacement results at the receivers as a function of time, these displacements are due to the P-, S- waves and the Rayleigh wave propagating along the surface as in the previous load type case. While we obtain similar errors in the solution of the P-wave using both the Bathe method and

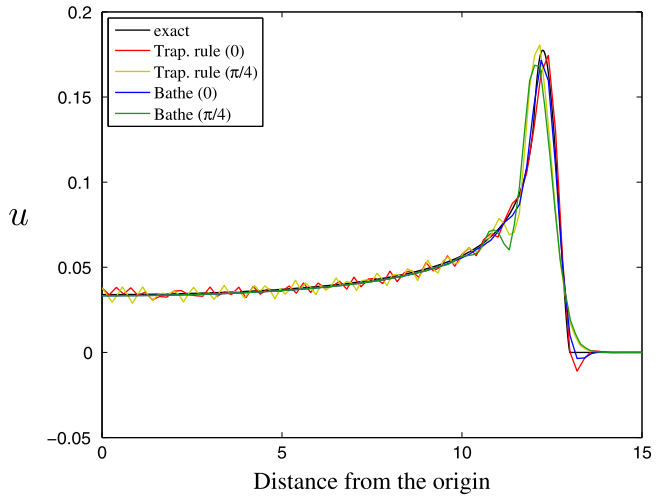

Fig. 18. Displacement variations along the various propagating angles, at time $t = 13$, 75 by 75 element mesh.

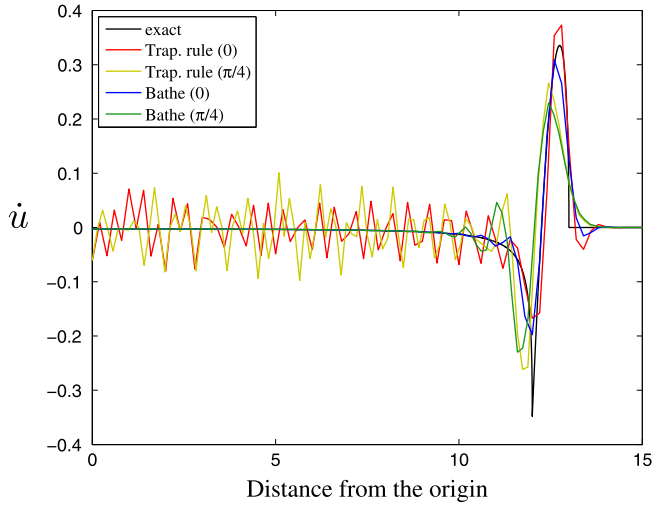

Fig. 19. Velocity variations along the various propagating angles, at time $t = 13$, 75 by 75 element mesh.

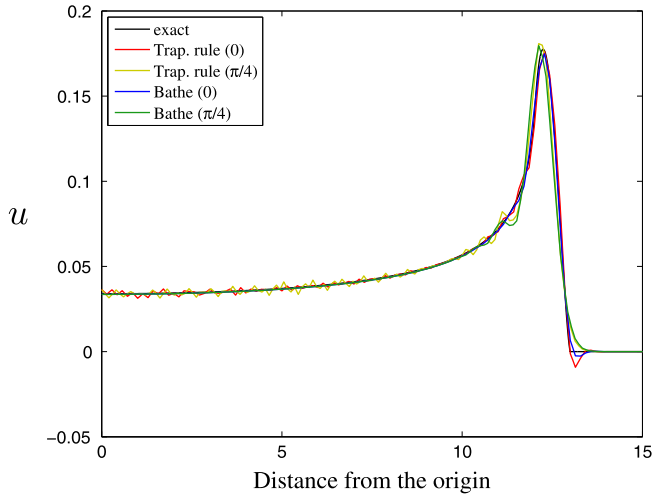

Fig. 20. Displacement variations along the various propagating angles, at time $t = 13$, 105 by 105 element mesh.

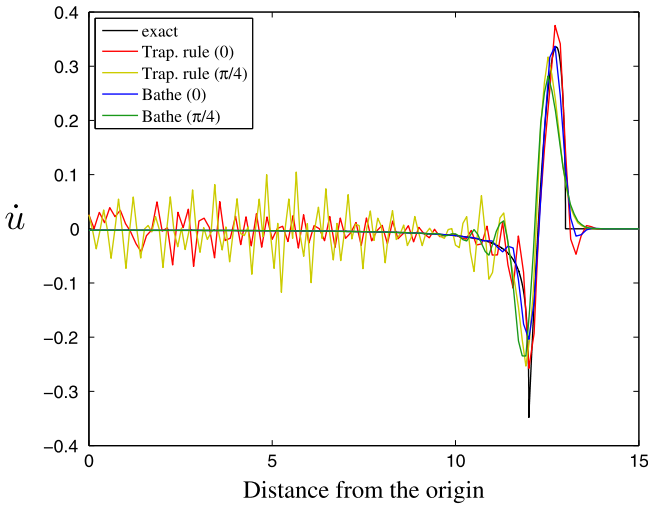

Fig. 21. Velocity variations along the various propagating angles, at time $t = 13$, 105 by 105 element mesh.

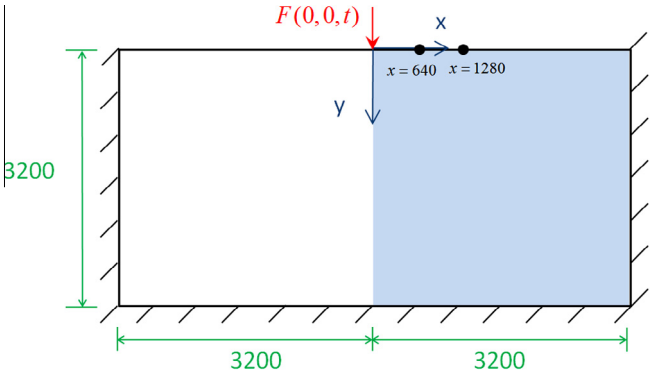

Fig. 22. A Lamb problem. $V_P = 3200$, $V_S = 1848$, $V_{\text{Rayleigh}} = 1671$. Two receivers are placed at $x = 640$ and $x = 1280$, computational domain is shaded.

the trapezoidal rule, as expected, the solution of the Rayleigh wave predicted using the trapezoidal rule has larger spurious oscillations than seen when using the Bathe method.

We can see the difference in the solution accuracy also when considering the predicted stress wave fields, as shown in Fig. 26, where it is seen that most of the energy is transported by the Rayleigh wave. We see that the stress waves are well predicted using the Bathe method but the solution using the trapezoidal rule shows in various areas undesirable spurious oscillations.

4. Concluding remarks

The objective in this paper was to present features and characteristics of the Bathe time integration method in the analysis of wave propagation problems, with emphasis on the effective use of the method to obtain solutions of optimal accuracy. We focused on how the direct time integration scheme significantly improves the solution by its property to suppress undesirable oscillations with the use of an effective CFL number (indeed, like in the solution of structural dynamics problems, see Ref. [3])

We studied the dispersion properties of the Bathe method in comparison with those of the widely used Newmark trapezoidal rule. Using an appropriate time step size (CFL number) for a given

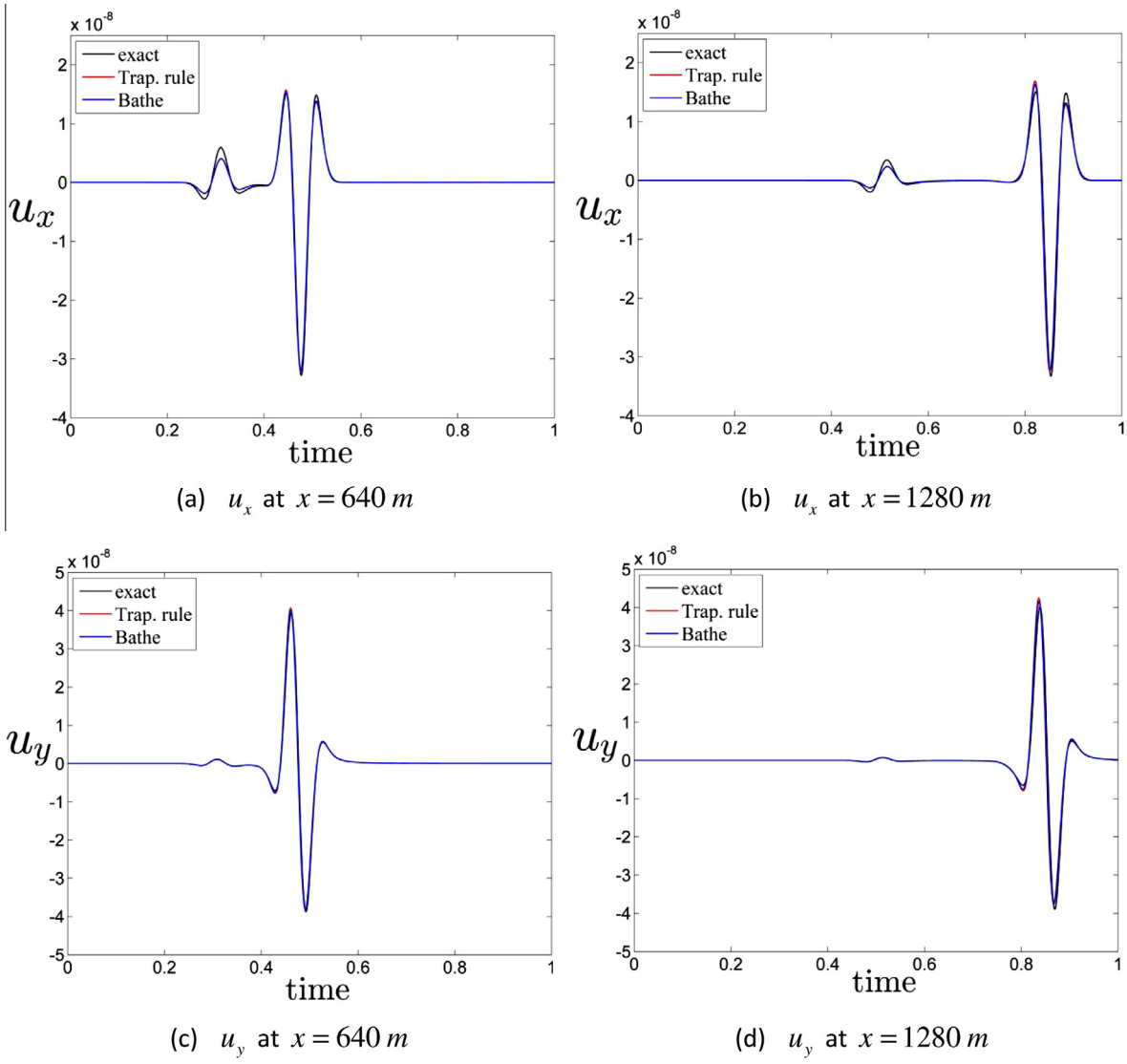

Fig. 23. Time history of displacement variations in *x*-direction and *y*-direction at the two receivers on the surface; Ricker wavelet line load.

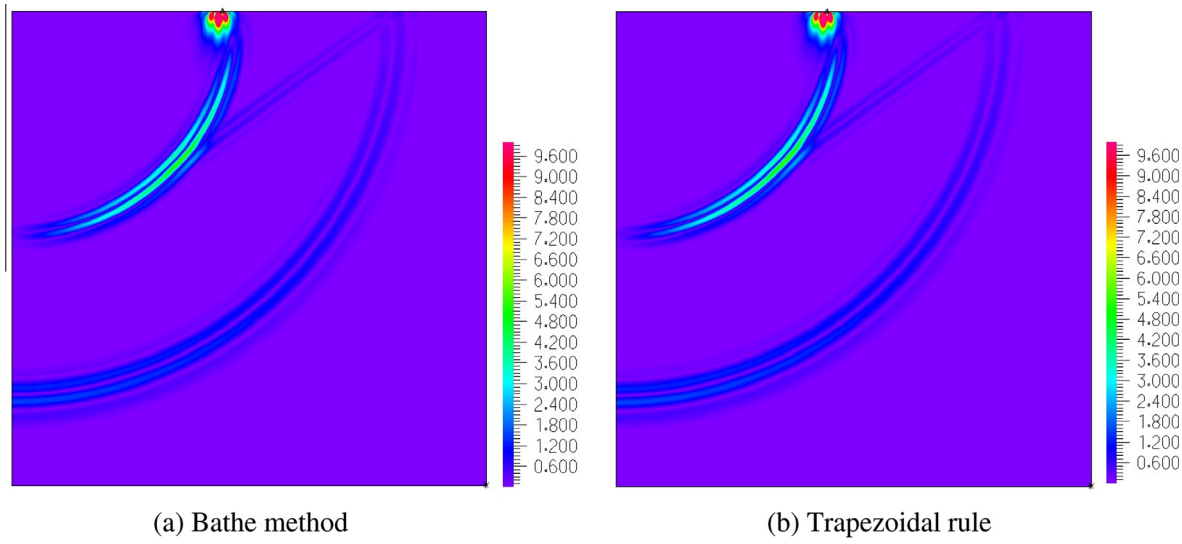

Fig. 24. Snapshots of von Mises stress at $t = 0.9196$ s; Ricker wavelet line load.

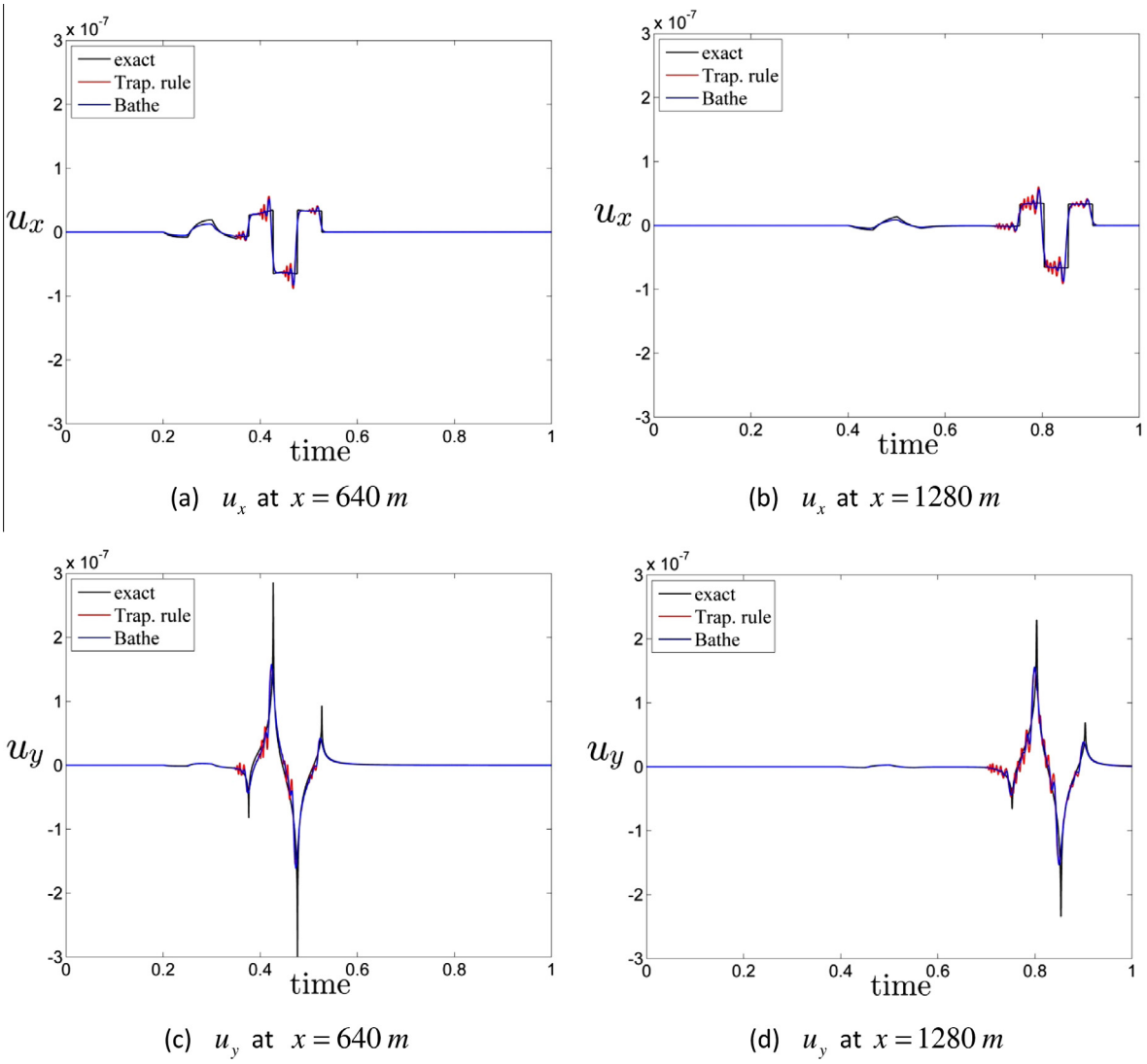

Fig. 25. Time history of displacement variations in the *x*- and *y*-directions at the two receivers on the surface; step functions line load.

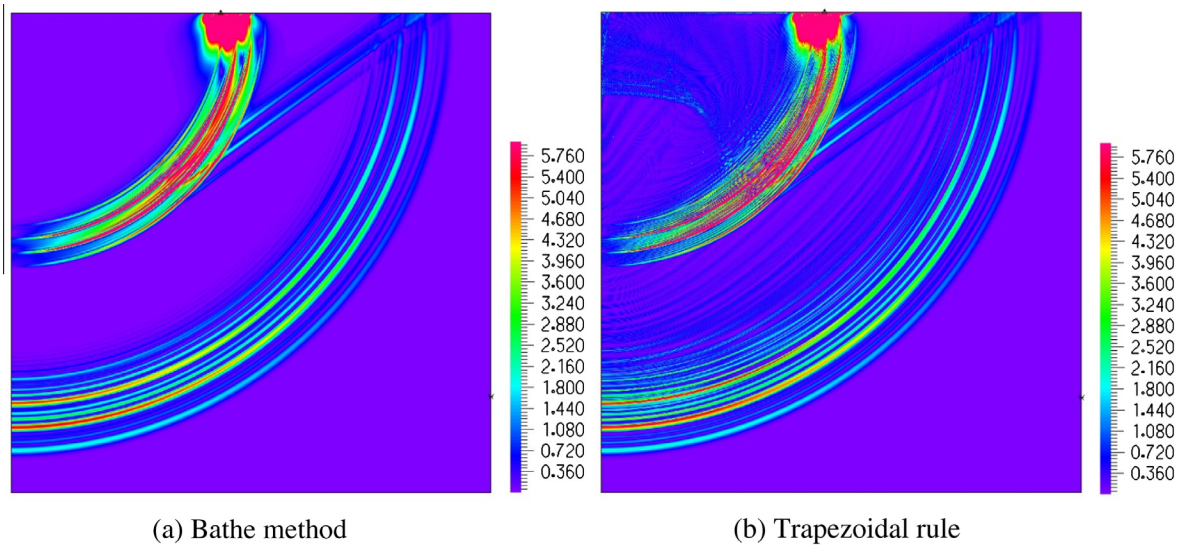

Fig. 26. Snapshots of von Mises stress at $t = 0.9196$ s; step functions line load.

mesh, the Bathe scheme calculates every wave accurately that can spatially be represented and does participate in the predicted response so that the total solution is almost non-dispersive. The waves that cannot be spatially represented are automatically discarded and therefore will not result into spurious oscillations, as found for example with the trapezoidal rule. It is important that the Bathe scheme does not require any additional treatment for wave propagation problems, and no numerical parameters are to be selected, like in the solutions of problems in structural dynamics.

However, whenever a wave propagation problem is solved, an appropriate spatial discretization is, of course, important. We considered here a very simple spatial discretization scheme and uniform meshes of simple geometries, because we wanted to focus on the basic characteristics of the time integration methods. Clearly, additional difficulties arise when the response in complex geometries is analysed using meshes in which distorted elements are present. Also, more powerful spatial discretizations should be considered, like higher-order elements [4] and enriched finite elements specifically constructed for the analysis of wave propagations [23]. While the conclusions of this paper will also be valuable in these cases, additional considerations will likely arise.

References

[1] Bathe KJ, Baig MMI. On a composite implicit time integration procedure for nonlinear dynamics. Comput Struct 2005;83:2513–24.
[2] Bathe KJ. Conserving energy and momentum in nonlinear dynamics: a simple implicit time integration scheme. Comput Struct 2007;85:437–45.
[3] Bathe KJ, Noh G. Insight into an implicit time integration scheme for structural dynamics. Comput Struct 2012;98–99:1–6.
[4] Bathe KJ. Finite element procedures. Prentice Hall; 1996.
[5] Tedesco JW, McDougal WG, Ross CA. Structural dynamics: theory and applications. Addison–Wesley; 1999.
[6] Chin RCY. Dispersion and Gibbs phenomenon associated with difference approximations to initial boundary-value problems for hyperbolic equations. J Comput Phys 1975;18:233–47.
[7] Boris JP, Book DL. Flux-corrected transport. 3. Minimal-error FCT algorithms. J Comput Phys 1976;20:397–431.
[8] Babuska I, Ihlenburg F, Strouboulis T, Gangaraj SK. A posteriori error estimation for finite element solutions of Helmholtz' equation. 2. Estimation of the pollution error. Int J Numer Methods Eng 1997;40:3883–900.
[9] Deraemaeker A, Babuska I, Bouillard P. Dispersion and pollution of the FEM solution for the Helmholtz equation in one, two and three dimensions. Int J Numer Methods Eng 1999;46:471–99.
[10] Babuska IM, Sauter SA. Is the pollution effect of the FEM avoidable for the Helmholtz equation considering high wave numbers? SIAM Rev 2000;42:451–84.
[11] Bao G, Wei GW, Zhao S. Numerical solution of the Helmholtz equation with high wavenumbers. Int J Numer Methods Eng 2004;59:389–408.
[12] Belytschko T, Mullen R. On dispersive properties of finite element solutions. In: Miklowitz J, Achenbach JD, editors. Modern problems in elastic wave propagation. John Wiley; 1978. p. 67–82.
[13] Wang YC, Murti V, Valliappan S. Assessment of the accuracy of the Newmark method in transient analysis of wave-propagation problems. Earthquake Eng Struct 1992;21:987–1004.
[14] Gottlieb D, Orszag SA. Numerical analysis of spectral methods: theory and applications. Capital City Press; 1993.
[15] Seriani G, Priolo E. Spectral element method for acoustic wave simulation in heterogeneous media. Finite Elem Anal Des 1994;16:337–48.
[16] Faccioli E, Maggio F, Paolucci R, Quarteroni A. 2D and 3D elastic wave propagation by a pseudo-spectral domain decomposition method. J Seismol 1997;1:237–51.
[17] Komatitsch D, Tromp J. Introduction to the spectral element method for three-dimensional seismic wave propagation. Geophys J Int 1999;139:806–22.
[18] Mahapatra DR, Gopalakrishnan S. A spectral finite element model for analysis of axial–flexural–shear coupled wave propagation in laminated composite beams. Compos Struct 2003;59:67–88.
[19] Karniadakis GE, Sherwin SJ. Spectral/hp element methods for computational fluid dynamics. Oxford University Press; 2005.
[20] Gamallo P, Astley RJ. The partition of unity finite element method for short wave acoustic propagation on non-uniform potential flows. Int J Numer Methods Eng 2006;65:425–44.
[21] Huttunen T, Gamallo P, Astley RJ. Comparison of two wave element methods for the Helmholtz problem. Commun Numer Methods Eng 2009;25:35–52.
[22] Kohno H, Bathe KJ, Wright JC. A finite element procedure for multiscale wave equations with application to plasma waves. Comput Struct 2010;88:87–94.
[23] Ham S, Bathe KJ. A finite element method enriched for wave propagation problems. Comput Struct 2012;94–95:1–12.
[24] Krieg RD, Key SW. Transient shell response by numerical time integration. Int J Numer Methods Eng 1973;7:273–86.
[25] Mullen R, Belytschko T. Dispersion analysis of finite element semidiscretizations of the two-dimensional wave equation. Int J Numer Methods Eng 1982;18:11–29.
[26] Foreman MGG. A two-dimensional dispersion analysis of selected methods for solving the linearized shallow-water equations. J Comput Phys 1984;56:287–323.
[27] Jiang L, Rogers RJ. Effects of spatial discretization on dispersion and spurious oscillations in elastic wave-propagation. Int J Numer Methods Eng 1990;29:1205–18.
[28] Cherukuri HP. Dispersion analysis of numerical approximations to plane wave motions in an isotropic elastic solid. Comput Mech 2000;25:317–28.
[29] Yue B, Guddati MN. Dispersion-reducing finite elements for transient acoustics. J Acoust Soc Am 2005;118:2132–41.
[30] Marfurt KJ. Accuracy of finite-difference and finite-element modeling of the scalar and elastic wave-equations. Geophysics 1984;49:533–49.
[31] Christon MA. The influence of the mass matrix on the dispersive nature of the semi-discrete, second-order wave equation. Comput Methods Appl Mech Eng 1999;173:147–66.
[32] Krenk S. Dispersion-corrected explicit integration of the wave equation. Comput Method Appl Mech Eng 2001;191:975–87.
[33] Seriani G, Oliveira SP. Optimal blended spectral-element operators for acoustic wave modeling. Geophysics 2007;72:95–106.
[34] Idesman AV, Schmidt M, Foley JR. Accurate finite element modeling of linear elastodynamics problems with the reduced dispersion error. Comput Mech 2011;47:555–72.
[35] Guddati MN, Yue B. Modified integration rules for reducing dispersion error in finite element methods. Comput Method Appl Mech Eng 2004;193:275–87.
[36] Holmes N, Belytschko T. Postprocessing of finite element transient response calculations by digital filters. Comput Struct 1976;6:211–6.
[37] Idesman A, Samajder H, Aulisa E, Seshaiyer P. Benchmark problems for wave propagation in elastic materials. Comput Mech 2009;43:797–814.
[38] Kuhl D, Crisfield MA. Energy-conserving and decaying algorithms in non-linear structural dynamics. Int J Numer Methods Eng 1999;45:569–99.
[39] Fung TC. Numerical dissipation in time-step integration algorithms for structural dynamic analysis. Prog Struct Eng Mater 2003;5:167–80.
[40] Bathe KJ. Advances in the multiphysics analysis of structures. In: Proceedings 11th international conference on computational structures technology, Dubrovnik, Croatia, Sept. 2012.
[41] Kazanci Z, Bathe KJ. Crushing and crashing of tubes with implicit time integration. Int J Impact Eng 2012;42:80–8.
[42] Wilson EL, Farhoomand I, Bathe KJ. Nonlinear dynamic analysis of complex structures. Earthquake Eng Struct 1973;1:241–52.
[43] Bathe KJ, Wilson EL. Stability and accuracy analysis of direct integration methods. Earthquake Eng Struct 1973;1:283–91.
[44] Bathe KJ. On reliable finite element methods for extreme loading conditions. In: Ibrahimbegovic A, Kozar I, editors. Chapter in extreme man-made and natural hazards in dynamics of structures. Springer; 2007.
[45] Payen DJ, Bathe KJ. A stress improvement procedure. Comput Struct 2012;112–113:311–26.